Science
AAAS

Widespread Persistent Thickening of the East Antarctic Ice Sheet by Freezing from the Base

Robin E. Bell, *et al.*

Science **331**, 1592 (2011);
DOI: 10.1126/science.1200109

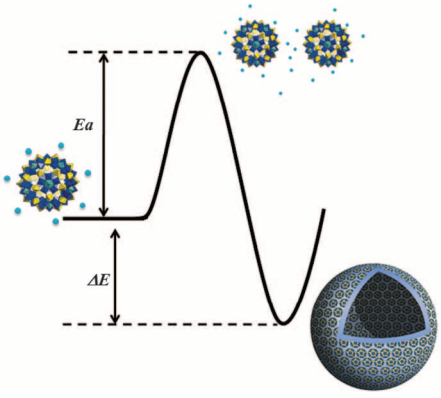

Fig. 3. Formal demonstration of the blackberry formation (see text).

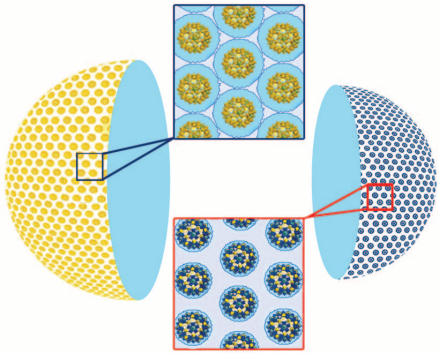

Fig. 4. Schematic plot demonstrating the different interfacial water mobilities (dynamical heterogeneities) of the $\{Mo_{72}Cr_{30}\}$ (yellow) and $\{Mo_{72}Fe_{30}\}$ (blue) blackberry-type assemblies. (Middle) The thick circle layer (blue) around the $\{Mo_{72}Cr_{30}\}$ clusters (top) illustrates stable, less mobile interfacial water compared to the $\{Mo_{72}Fe_{30}\}$ scenario (bottom). The average intermacroion distance related to the interfacial water is ~0.9 ± 0.4 nm (*13*).

with fig. S1) is slower than that through the $\{Mo_{72}Fe_{30}\}$-type system by a factor of 3 to 4 (*27*). Furthermore, the importance of hydrogen bonding for the superstructure formation is confirmed by the larger $\{Mo_{72}Fe_{30}\}$-type structures formed in H_2O compared with those in D_2O (25 nm versus 14 nm, figs. S2 and S3a) and the much slower process in D_2O (fig. S3b).

To rule out the possibility that the self-recognition is primarily due to kinetic effects (i.e., that one type of Keplerates assembles faster), we analyzed the kinetics of the assembly processes by static light scattering. Our results showed that the two assembly processes occur at almost the same speed (fig. S3), especially in the initial stages (fig. S4). The kinetic curves obtained can approximately be explained by a two-step nucleation-growth process: (i) the macroanions slowly associate into thermodynamically unfavorable intermediate oligomers and dimers; (ii) when enough oligomers of appropriate shape and metal content are present, formation of the two different blackberries is accelerated (*21*, *22*).

The two Keplerate materials investigated have a very broad range of interest for materials science (*7*, *11*), e.g., as molecular models for Kagomé lattices (*28*), as well as for quasi-crystals (*29*), and for geochemical processes regarding the modeling of H_2O exchange at iron minerals' surfaces (*30*).

References and Notes

1. J.-M. Lehn, *Supramolecular Chemistry: Concepts and Perspectives* (VCH, Weinheim, Germany, 1995).
2. R. Jelinek Ed., *Cellular and Biomolecular Recognition: Synthetic and Non-Biological Molecules* (Wiley-VCH Weinheim, Germany, 2009).
3. We refer to self-recognition here (in context with the present assembly process leading to phase separation) according to the definition: "Self-assembly may occur with *self-recognition*, mixtures of components yielding defined superstructures without interference or crossover" [(*1*), p. 142].
4. A. Müller *et al.*, *Angew. Chem. Int. Ed.* **38**, 3238 (1999).
5. A. M. Todea *et al.*, *Angew. Chem. Int. Ed.* **46**, 6106 (2007).
6. D.-L. Long, L. Cronin, *Chemistry* **12**, 3698 (2006).
7. A. Proust, R. Thouvenot, P. Gouzerh, *Chem. Commun. (Camb.)* **2008**, 1837 (2008).
8. A. Müller, S. Roy, in *The Chemistry of Nanomaterials: Synthesis, Properties and Applications*, C. N. R. Rao, A. Müller, A. K. Cheetham, Eds. (Wiley-VCH, Weinheim, Germany, 2004), pp. 452–475.
9. N. Hall, *Chem. Commun. (Camb.)* **2003** (no. 7), 803 (2003) (Focus Article).
10. D.-L. Long, E. Burkholder, L. Cronin, *Chem. Soc. Rev.* **36**, 105 (2007).
11. A. Müller, S. Roy, *J. Mater. Chem.* **15**, 4673 (2005).
12. T. Liu, *J. Am. Chem. Soc.* **124**, 10942 (2002).
13. T. Liu, *J. Am. Chem. Soc.* **126**, 406 (2004).
14. T. Liu, *Langmuir* **26**, 9202 (2010).
15. M. L. Kistler, T. Liu, P. Gouzerh, A. M. Todea, A. Müller, *Dalton Trans.* **26**, 5094 (2009).
16. A. Müller *et al.*, *Chem. Commun. (Camb.)* **19**, 1928 (2001).
17. T. Liu, E. Diemann, H. Li, A. W. M. Dress, A. Müller, *Nature* **426**, 59 (2003).
18. M. L. Kistler, A. Bhatt, G. Liu, D. Casa, T. Liu, *J. Am. Chem. Soc.* **129**, 6453 (2007).
19. S. W. Provencher, *Biophys. J.* **16**, 27 (1976).
20. Materials and methods are available as supporting material on *Science* Online.
21. J. Zhang, D. Li, G. Liu, K. J. Glover, T. Liu, *J. Am. Chem. Soc.* **131**, 15152 (2009).
22. G. Liu, T. Liu, *Langmuir* **21**, 2713 (2005).
23. E. Fratini, A. Faraone, A. M. Todea, P. Baglioni, *Inorg. Chim. Acta* **363**, 4234 (2010).
24. A. Zlotnick, J. M. Johnson, P. W. Wingfield, S. J. Stahl, D. Endres, *Biochemistry* **38**, 14644 (1999).
25. F.-C. Xu, H. R. Krouse, T. W. Swaddle, *Inorg. Chem.* **24**, 267 (1985).
26. J. Holzmann, A. Appelhagen, R. Ludwig, *Z. Phys. Chem.* **223**, 1001 (2009).
27. P. P. Mishra, J. Pigga, T. Liu, *J. Am. Chem. Soc.* **130**, 1548 (2008).
28. I. Rousochatzakis, A. M. Läuchli, F. Mila, *Phys. Rev. B* **77**, 094420 (2008).
29. A. Müller, *Nat. Chem.* **1**, 13 (2009).
30. E. Balogh, A. M. Todea, A. Müller, W. H. Casey, *Inorg. Chem.* **46**, 7087 (2007).

31. T.L. acknowledges support of this work by the National Science Foundation, Lehigh University, and the Alfred P. Sloan Foundation. A.M. acknowledges the continuous support of the Deutsche Forschungsgemeinschaft.

Supporting Online Material

www.sciencemag.org/cgi/content/full/331/6024/1590/DC1
Materials and Methods
Figs. S1 to S5
References

1 December 2010; accepted 11 February 2011
10.1126/science.1201121

Widespread Persistent Thickening of the East Antarctic Ice Sheet by Freezing from the Base

Robin E. Bell,[1] Fausto Ferraccioli,[2] Timothy T. Creyts,[1] David Braaten,[3] Hugh Corr,[2] Indrani Das,[1] Detlef Damaske,[4] Nicholas Frearson,[1] Thomas Jordan,[2] Kathryn Rose,[2] Michael Studinger,[5] Michael Wolovick[1]

An International Polar Year aerogeophysical investigation of the high interior of East Antarctica reveals widespread freeze-on that drives substantial mass redistribution at the bottom of the ice sheet. Although the surface accumulation of snow remains the primary mechanism for ice sheet growth, beneath Dome A, 24% of the base by area is frozen-on ice. In some places, up to half of the ice thickness has been added from below. These ice packages result from the conductive cooling of water ponded near the Gamburtsev Subglacial Mountain ridges and the supercooling of water forced up steep valley walls. Persistent freeze-on thickens the ice column, alters basal ice rheology and fabric, and upwarps the overlying ice sheet, including the oldest atmospheric climate archive, and drives flow behavior not captured in present models.

Large ice sheets thicken by the accumulation of snow on the surface, yet little is known about processes at the base of the ice sheets. Radar images of ice sheets are characterized by isochronous internal layers associated with changes in the dielectric properties of

the ice. In the center of ice sheets, these internal layers continue almost to the ice sheet bed (*1*). Away from the domes and ice divides, these layers disappear in the bottom 10 to 30% of the ice sheet. This homogeneous, echo-free basal layer can be hundreds of meters thick (*2*) and is considered to be the result of elevated basal temperatures, deformed ice, stagnant ice, or increased layer roughness (*3*). The absence of reflectors in the base of the ice sheet makes decoding basal processes difficult. In a few locations, near-bed reflectors have been resolved in the echo-free zone, specifically surrounding subglacial mountain peaks east of Dome Fuji (*4*) and over Lake Vostok (*5*). Over Lake Vostok, these reflectors are associated with frozen-on lake water sampled in the 5G Borehole (*6*) and are attributed to changing fabric in the basal ice (*6*).

During the International Polar Year 2007–2009, the seven-nation Antarctica's Gamburtsev Province (AGAP) expedition sought to comprehensively image the ice sheet bed, deep in the interior of Antarctica (*7*). This study used airborne and ground-based geophysical methods to understand the fundamental structure of Dome A, the top of the East Antarctic ice sheet and the underlying Gamburtsev Mountains (Fig. 1). The Gamburtsev Mountains were a major nucleation point for growth of the Antarctic ice sheet during the Cenozoic (*8*). Presently, ice at Dome A drains into all the major ice shelves of Antarctica. Processes occurring in the Dome A region have the potential to affect the majority of East Antarctica. Two Twin Otter aircraft were equipped with ice-penetrating radars, laser ranging systems, gravity meters, and magnetometers. The main survey grid included north-south lines spaced 5 km apart, with crossing lines every 33 km. 150-MHz ice-penetrating radars with bandwidths of 15 to 20 MHz produced high-resolution images of the internal structure of the East Antarctic ice sheet.

Beneath Dome A, the internal layers extend close to the base of the ice sheet, whereas away from the dome, the bottom ~1000 m of the ice sheet becomes echo-free. Using improved radar technologies, we have imaged distinct near-bed reflectors within the generally echo-free zone. There appear to be two populations of near-bed reflectors, one found adjacent to the high ridges of the Gamburtsev Subglacial Mountains and one found along the steep valley walls.

The first population of basal reflectors originates along the high ridges at the valley heads (Fig. 1B). Valley heads are the upstream terminus of the Gamburtsev Mountain valley network. Bright horizontal bed reflectors indicate that subglacial water collects at these valley heads. The basal reflectors separate from the bright, water-filled ice sheet bed, similar to the divergence of the freeze-on reflector over Lake Vostok. The coherence of these reflectors over adjacent lines confirms that these near-bed reflectors are not artifacts of off-nadir reflections. The origin and lateral extent of these reflectors are best illustrated with radar data along ice flow (Fig. 2, A and B). The valley head basal reflectors can be traced for 50 to 100 km along flow lines (Fig. 1, A to C).

[1]Lamont-Doherty Earth Observatory of Columbia University, Palisades, NY 10964, USA. [2]British Antarctic Survey, High Cross, Madingley Road, Cambridge CB3 0ET, UK. [3]Center for the Remote Sensing of Ice Sheets, Kansas University, Lawrence, KS, USA. [4]Bundesanstalt für Geowissenschaften und Rohstoffe, Hannover, Germany. [5]Goddard Earth Science and Technology Center, University of Maryland Baltimore County, MD, and NASA Goddard Space Flight Center, MD, USA.

*To whom correspondence should be addressed. E-mail: robinb@ldeo.columbia.edu

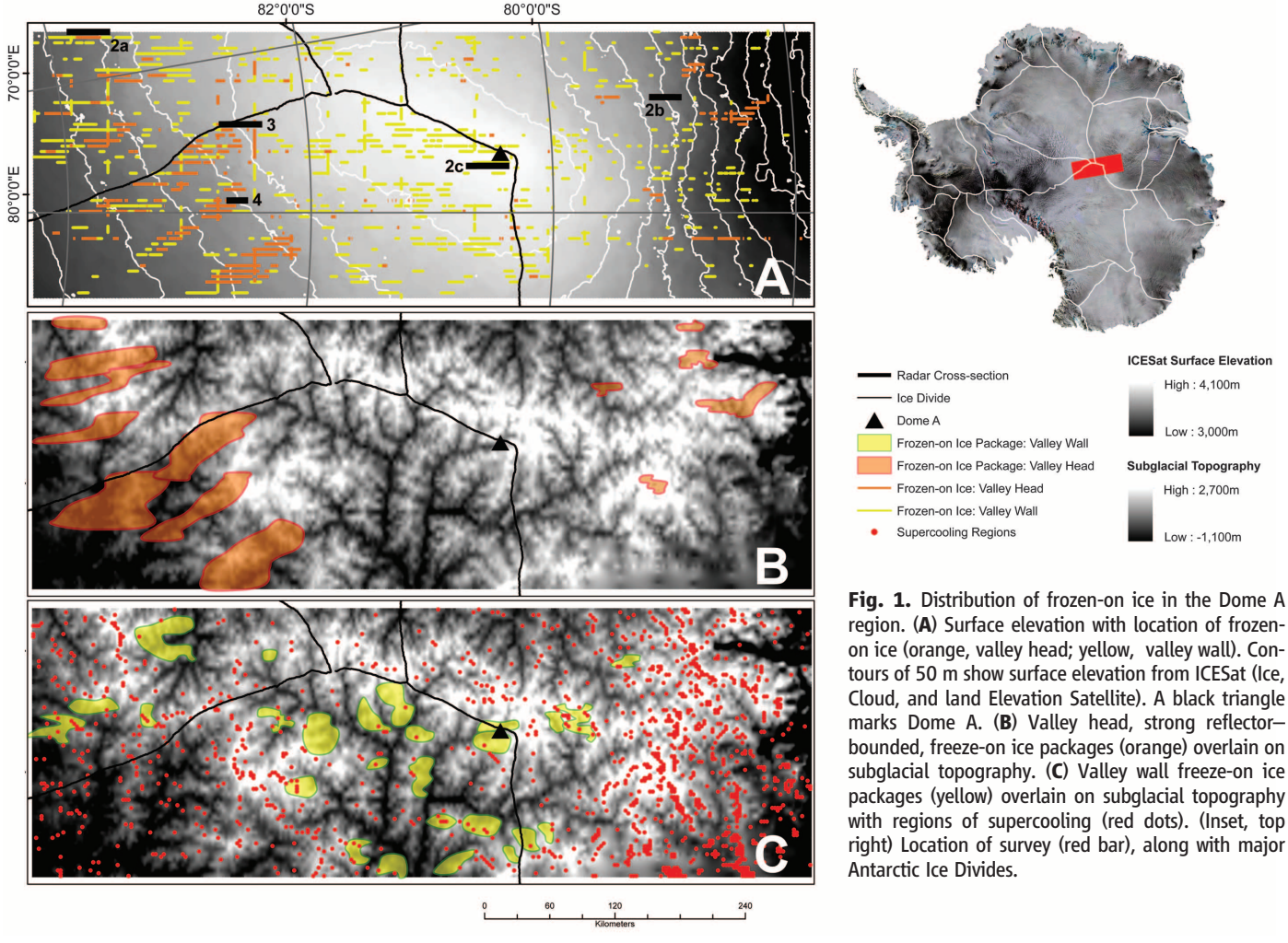

Fig. 1. Distribution of frozen-on ice in the Dome A region. (**A**) Surface elevation with location of frozen-on ice (orange, valley head; yellow, valley wall). Contours of 50 m show surface elevation from ICESat (Ice, Cloud, and land Elevation Satellite). A black triangle marks Dome A. (**B**) Valley head, strong reflector–bounded, freeze-on ice packages (orange) overlain on subglacial topography. (**C**) Valley wall freeze-on ice packages (yellow) overlain on subglacial topography with regions of supercooling (red dots). (Inset, top right) Location of survey (red bar), along with major Antarctic Ice Divides.

The near-bed reflector amplitude is stronger than the return from ice sheet internal layers but weaker than the return from the ice sheet bed. The valley head reflectors are often laminated. Downflow, these reflectors become fragmented and disappear into the background noise of the echo-free zone. We have identified 12 distinct packages of ice bounded by these bright basal reflectors (Fig. 1B). In the Dome A region, ~7% of the base of the ice sheet is characterized by packages of valley head ice. These valley head packages originate where the ice sheet is 2400 to 3000 m thick. The ice package widths range from 2 to 25 km, and the average thickness is ~490 m. The maximum package thickness is 1100 m, where the basal ice constitutes 50% of the ice sheet. The estimated frozen-on ice volume of the basal ice packages ranges from 45 to 1064 km^3.

The second population of basal reflectors is found primarily along the steep valley walls of the Gamburtsev Mountains. These reflectors define 200- to 500-m-thick packages that drape the downflow side of steep valley walls (Fig. 2C). The valley wall packages have a relatively weak upper reflector underlain by a uniform distribution of point reflectors with no distinct laminations. On the south side of Dome A, ~16% of the base of the ice sheet is characterized by these reflectors. The average thickness of the 24 packages of ice (Fig. 1B) defined by these diffuse reflectors is 350 m. The packages of ice can be traced for 15 to 30 km along the flow direction and have volumes of up to 160 km^3.

We interpret both populations of basal reflectors and the underlying packages of ice as the result of basal freeze-on. The volume of ice frozen on to the base of the ice sheet at the Gamburtsev Mountains' valley heads is 8600 km^3. The total volume of the valley wall freeze-on ice is ~3900 km^3. We can use the 1.7 m/year surface velocity measured at the AGAP field camp at the southern margin of the study area and the along-flow length of these packages to estimate a minimum age for the process. Using this simple approach, the valley head freeze-on process has been persistent for a minimum of 30,000 to 60,000 years, whereas the valley wall freeze-on has been persistent for a minimum of 10,000 to 20,000 years. The process of basal freeze-on has continued through the glacial-interglacial transition. The processes are likely to have been persistent for substantially longer, but older freeze-on ice may not be easily detected by radar. In the southern Dome A region, 27,000 km^2 of the 125,500 km^2 area surveyed consists of freeze-on ice. A minimum of 24% of the ice sheet base is affected by the freeze-on process.

The two populations of basal ice are distinct in the strength of the upper reflector, the structure of the underlying package of ice, and their geographic distribution. There are two possible freeze-on mechanisms (*9*): conductive cooling or glaciohydraulic supercooling (*10*). We suggest that the two populations of basal reflectors reflect the two freeze-on mechanisms. These processes are illustrated diagrammatically in Fig. 3B. The valley head basal ice packages are consistently sourced from ponded subglacial water along the mountain ridges. Along these ridges, where the overlying ice sheet is thin, cold, and has steep thermal gradients, conductive cooling is the dominant process. The conductive cooling over ponded water may cause fractionation of the water chemistry during freeze-on and loss of the sediment load as the water ponds. Fractionation and sediment loss over ponded water are the probable source of the laminations in the valley head packages. Conductive cooling is probably the primary mechanism responsible for the freeze-on ice at the valley heads, whereas supercooling is likely to be a more rapid process when subglacial water actively moves up steep slopes. As compared to ice frozen-on from a conductively cooling subglacial water body, supercooled ice will have experienced less chemical fractionation or segregation of the suspended sediments. A supercooled package of ice is therefore likely to be a more homogenous basal package. Most of the valley wall units are associated with locations where the supercooling threshold

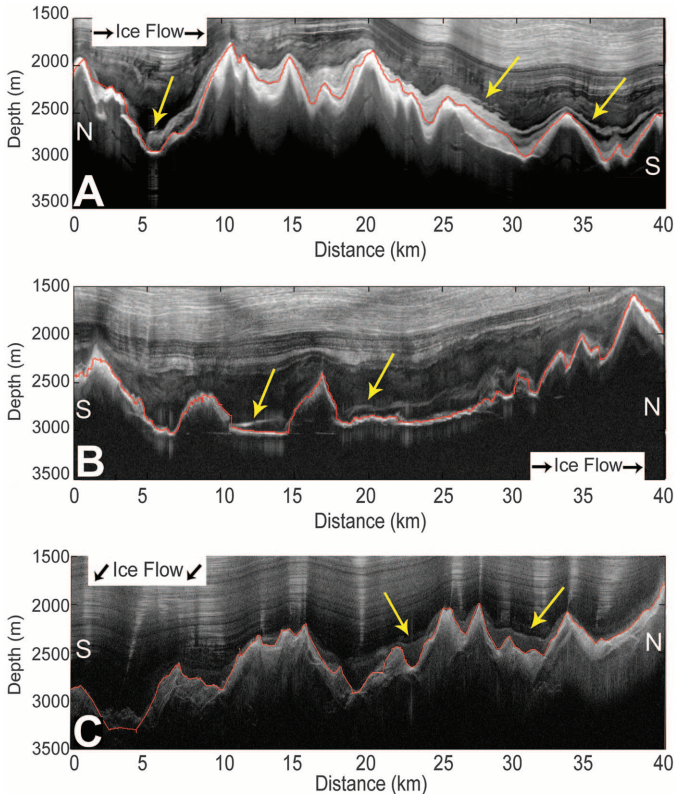

Fig. 2. Radar images of type examples of valley head (**A** and **B**) and valley wall freeze-on ice (**C**). (C) is in the valley beneath the Chinese Kunlun Station at Dome A. The location of these profiles is shown in Fig. 1. The base of the ice sheet (bed) is marked in red. The top of the frozen-on ice is indicated with yellow arrows.

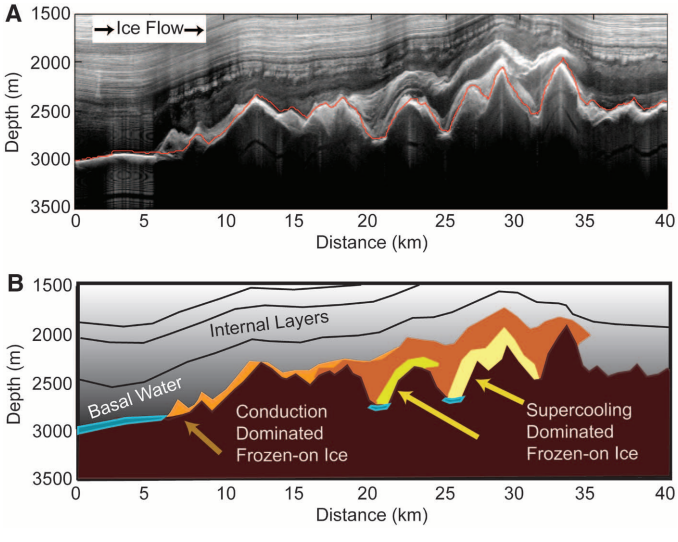

Fig. 3. Freeze-on processes. (**A**) Radar image. (**B**) Schematic of freeze-on processes. The location of this profile is shown in Fig. 1.

has been exceeded (Fig. 1C). We suggest that the valley wall packages are the result of supercooling of subglacial water moving over rough basal topography. The freeze-on at the valley heads is primarily the result of conductive cooling over static bodies of water, whereas the valley wall ice is primarily the result of the hydrologic potential forcing water up steep valley slopes. Because these processes are not mutually exclusive, individual packages of frozen-on ice are likely to have been produced by a combination of the two mechanisms. Alternative mechanisms for producing the contrasting radar signatures found within the frozen-on ice include spatial and temporal changes in basal water availability or chemistry.

The addition of hundreds of meters of ice to the base of an ice sheet deforms the overlying ice upward. This upwarping modifies the ice sheet stratigraphy and may affect the surface accumulation by changing the surface slope. The thickest package of frozen-on ice (1110 m) is situated at the downflow end of a 20-km-long valley floored by a bright horizontal reflector. The internal layers are deformed upward over 410 m at the valley head, conforming to the shape of the accreted ice body and not the underlying topography (Fig. 4). The accretion sites in the Dome A region are typically coincident with 5- to 35-m mounds in the ice surface, indicating linkage between the basal processes and the ice surface morphology.

The thick packages of freeze-on ice surrounding Dome A illustrate that basal freeze-on modifies the fundamental structure of ice sheets, thickening the ice column from the base. The freeze-on rates in the Dome A region may be locally greater than the surface accumulation rates. The upwarping of internal layers over accretion sites implies active interaction between basal accretion and the entire ice sheet. The accretion-induced upwarping of basal ice will move old ice to a higher elevation in the ice sheet, increasing the potential of preserving very old ice. Alternatively, the widespread melt required to support the freeze-on process may have destroyed the ice containing the ancient paleoclimate records. Without the inclusion of basal processes, simple models of ice sheet temperatures cannot accurately predict the location of the oldest ice (*11*).

In East Antarctica, basal freeze-on has continued in the same locations through the last glacial-interglacial transition and has probably been a persistent process since East Antarctica became encased in a large ice sheet 32 million years ago. The simple geometry of the subglacial topography and the stable ice flow in the Dome A region have enabled us to image this process for the first time. Although the surface accumulation, surface slope, and bed morphology vary distinctly on the northern and southern sides of Dome A, throughout the area almost a quarter of the ice sheet base consists of ice freeze-on from the bottom. Widespread freeze-on can change the rheology and modify the flow of the Antarctic and Greenland ice sheets (*12*, *13*). Inclusion of these basal processes is essential to produce robust predictions of future ice sheet change.

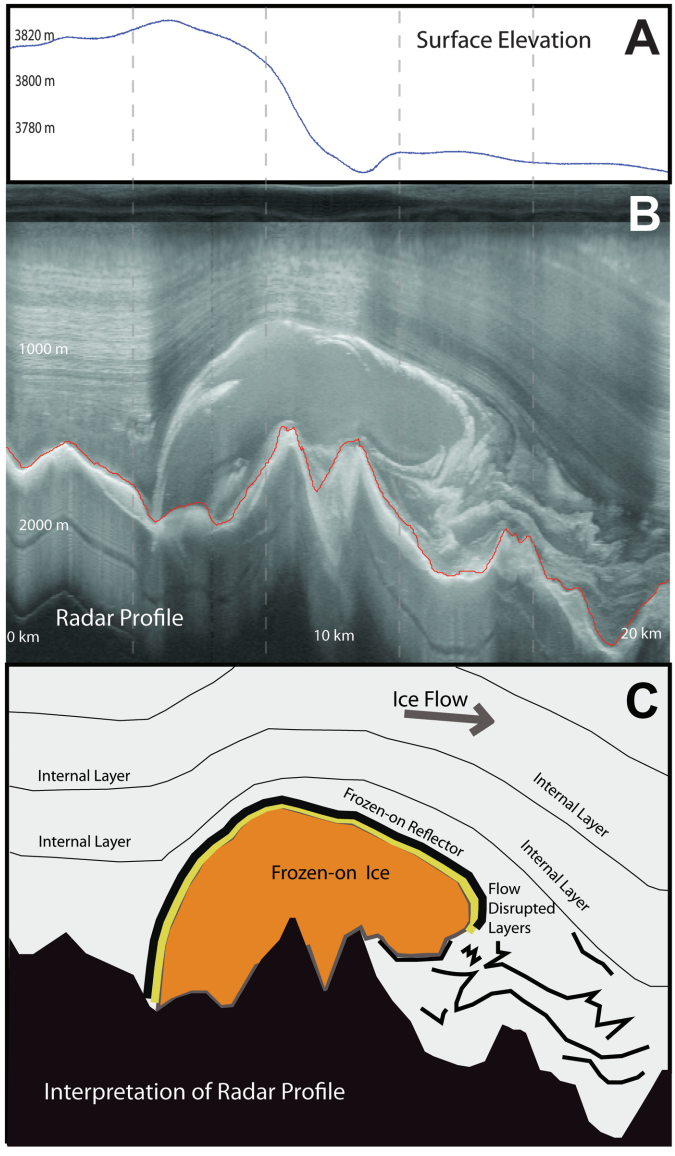

Fig. 4. AGAP radar and lidar data over the freeze-on ice package (Fig. 1). (**A**) is the airborne scanning laser profile over the freeze-on ice. The ice surface along this profile is 5 m above the regional slope, whereas on the two upstream lines, a 10- to 15-m mound in the ice surface is coincident with the sites of freeze-on. The radar profile (**B**) illustrates the upward deflection of the internal layers over the accretion site. The accretion plume is 1100 m thick along this profile, and the internal layers are deflected upward 400 m. (**C**) illustrates the upward deflection of the internal layers. The location of the profile is shown in Fig. 1.

References and Notes

1. G. Q. Robin, C. W. M. Swithinbank, B. M. E. Smith, *Radio Echo Exploration of the Antarctic Ice Sheet* (International Association of Scientific Hydrology Publication 86, 1970), pp. 97–115.
2. G. De Q. Robin, D. J. Drewry, D. T. Meldrum, *Philos. Trans. R. Soc. London Ser. B* **279**, 185 (1977).
3. R. Drews *et al.*, *Cryosphere* **3**, 195 (2009).
4. S. Fujita *et al.*, *J. Geophys. Res.* **104**, 13013 (1999).
5. R. E. Bell *et al.*, *Nature* **416**, 307 (2002).
6. J. A. MacGregor, K. Matsuoka, M. Studinger, *Earth Planet. Sci. Lett.* **282**, 222 (2009).
7. R. E. S. Bell *et al.*, paper presented at the 2009 Full Meeting of the American Geophysical Union, San Francisco, CA, 14 to 18 December 2009.
8. R. M. DeConto, D. Pollard, *Nature* **421**, 245 (2003).
9. T. T. Creyts *et al.*, paper presented at the 2010 Fall Meeting of the American Geophysical Union, San Francisco, CA, 13 to 17 December 2010.
10. R. B. Alley, D. E. Lawson, E. B. Evenson, J. C. Strasser, G. J. Larson, *J. Glaciol.* **44**, 563 (1998).
11. F. Pattyn, *Earth Planet. Sci. Lett.* **295**, 451 (2010).
12. F. Heliere, L. Chung-Chi, H. Corr, D. Vaughan, *IEEE Trans. Geosci. Remote Sensing* **45**, 2573 (2007).
13. D. E. Sugden *et al.*, *Nature* **328**, 238 (1987).

14. We acknowledge the seven nations involved in the AGAP International Polar Year effort for their logistical, financial, and intellectual support. Specifically, the U.S. Antarctic Program of NSF provided support for the logistics, the development of the instrumentation, and the analysis of the data. The Natural Environment Research Council/British Antarctic Survey provided extensive support for deep-field logistics, data collection, and analysis. The Federal Institute for Geosciences and Resources, Germany, and the Polar Research Institute of China provided invaluable support to the program. C. Finn, Gwenn Flowers, M. Fahnestock, and Slawek Tulaczyk provided early reviews of the work. H. Abdi provided technical support in developing the figures.

8 November 2010; accepted 18 February 2011
Published online 3 March 2011;
10.1126/science.1200109